Additional Tools for Locating and Quantifying a Range's Stray Signals

Scott T. McBride
NSI-MI Technologies
Suwanee, GA USA
Scott.McBride@Ametek.com

***Abstract*— Earlier works have shown the benefits of imaging stray signals in a range with planar-scanner data. This paper discusses some additional tools that can be employed for stray-signal identification. Related range diagnostics are presented that employ Fourier spectral and holographic processing of 1D linear scans through the quiet zone. For the special case of a compact range, the interpretation of arrival angles from the paraboloidal reflector surface is explored. Measured data from multiple facilities are presented that were used to locate, quantify, and remedy the unwanted signals.**

Keywords: stray signals, range imaging, field probing, spectral analysis, microwave holography

I. Introduction

The most common evaluation of a new compact or far-field range is a field-probing activity, with horizontal and vertical centerline scans acquired through the quiet zone (QZ). Amplitude taper and field ripple are quantified in each scan and compared to specifications. Excessive QZ ripple, typically caused by unwanted reflections, can indicate "we have a problem," but will rarely suggest "here's what you need to fix."

If an x-y planar scanner is available in the QZ, then algorithms exist[1] to turn a regular x-y grid of QZ amplitudes and phases into an image showing directions toward and magnitudes of stray signals within the range. Similar algorithms[2][3] can produce an equivalent image from a regular polar grid, but the amount of acquired data and axis-alignment fidelity needed for a quality image often make this impractical. In many facilities where the plane-polar acquisition was performed, nearly all of the excessive ripple was captured in the one vertical cut. This paper therefore includes two algorithms for processing individual diametric cuts through the QZ to help locate and quantify stray signals.

The first algorithm, in Section III, is the 1D version of the 2D mapping in [1]. It simply does a fast Fourier transform (FFT) of the single scan's measured data, plots the output vs. angle, and optionally calls for overlays of expected angles to suspect range features. The second algorithm, in Section IV, does iterative microwave holography[4] of the single scan, propagating radially away from the line where it was measured (presumably back toward the range antenna), producing a spatial-domain image of the estimated field strength vs. propagation radius and scan-axis position.

It is commonly known that a compact range's paraboloidal reflector will turn a spherical wave emanating from the focal point into a plane wave propagating parallel to the paraboloid's axis. Conversely, a plane wave at the QZ with an angle of arrival (AoA) parallel to the range axis corresponds to a spherical wave from the focal point. The conversion of an arbitrary reflector-to-QZ AoA into the corresponding scatterer-to-reflector AoA, however, seems much less commonly understood. Section II discusses the relevant paraboloidal ray tracing, giving an easy conversion that is sufficient to find most scatterers, and suggests the basis for a more rigorous calculation should it be needed. Section II is applicable to any algorithm, including those in [1], [3], Section III, and Section IV, that reports stray signals in directions toward a paraboloidal reflector.

Sections III and IV show examples for compact ranges. Note, however, that these algorithms are suitable for any range geometry where linear scans are available in the test zone. The plane-wave subtraction used in these examples, if needed, will not be as straightforward if the desired signal is not a plane wave.

II. Tracing Rays Through a Paraboloidal Reflector (or "Through the Fun-House Mirror")

The focal point of a compact-range reflector can often be a crowded place, with positioner(s) and feed(s) and absorber treatment(s). Achieving high-quality absorber treatment there is frequently both crucial and difficult.

When imaging field-probe data, either with [1] or in Section III, to find stray signals' AoAs, some of those angles may point toward the reflector. When this is the case, the root cause might be the reflector surface or edge treatments, or it might instead be something whose unwanted signal bounces off the reflector. This section deals with the latter possibility, discussing how to estimate the scattering source's location from the reflected wave's QZ AoA.

Figure 1 shows a photograph taken from the QZ of a small blended-rolled-edge reflector, with a paper target placed near the feed. The paper target has a regular square grid with equal horizontal and vertical spacing. This reflector has been polished in its central region, and the paraboloid starts blending to the rolled edges just outside that central area. Still, this photo might help provide some high-level understanding about the paraboloid's reflection of off-focal-point sources. In Figure 1 we see very little distortion of the square grid within the reflector's paraboloidal section.

Figure 1 Photo of paper-target grid just behind feed through polished rolled-edge reflector.

One of many differences between this image and what would be seen through a planar mirror is the apparent size of the feed and paper target. With a planar mirror, the paper target's grid spacing would appear to get smaller with increasing observation distance from the mirror. With the paraboloidal mirror, the angular spacing of that grid remains constant with observation distance. Since the angular span of the reflector gets smaller with increasing observation distance, there's an illusion that the grid grows larger. Another difference is in the response to translating the observation point in X and/or Y. With a planar mirror, such a translation would change the angle at which the paper target appears. With a paraboloid, the look angle to the focal point's reflection is always parallel to the Z axis, so the paper-target image appears to translate with the observation point.

A. Mapping from Known Angle of Arrival

Figure 2 illustrates the ray-tracing optics of a paraboloid. The commonly understood ray tracing is shown with the dashed (black) line, where all rays from the focal point are parallel and nominally horizontal heading toward the QZ. The reflector's local normal at any location bisects the incident and reflected angle, as shown in Figure 2 as two thin blue lines.

Signals emanating from locations other than the focal point also reflect symmetrically about each local normal on the paraboloid. For other locations near the focal point and especially in the focal plane[5] (the plane through the focal point whose normal points to the reflector center), the resulting field is an approximate plane wave arriving from a different direction. For a true plane wave, all reflected rays would be parallel. Figure 2 has contrived the scatterer's location to make those rays nearly parallel to simplify the initial discussion.

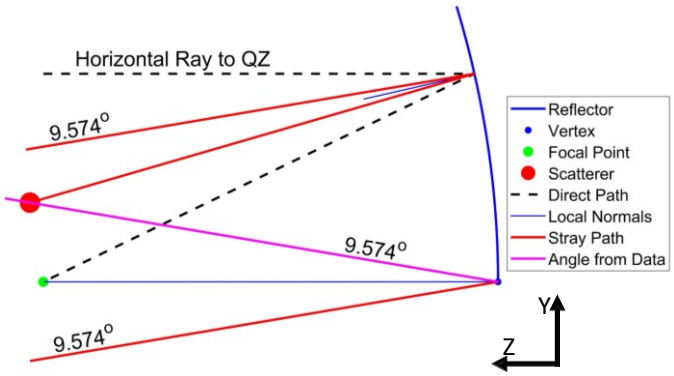

Figure 2 Paraboloidal ray-tracing illustration.

At the upper left of Figure 2 is a ray toward the QZ annotated with "9.574°". This angle would have been determined as an elevation AoA from 1D (described in Section III) or 2D[1] spectral processing. Our goal here is to determine where that would originate if we assume that the signal bounced off the paraboloidal reflector.

The easiest approximation, which works well for sources near the feed and many that aren't, is to assume the stray signal is a true plane wave. This implies that all rays heading toward the extended QZ plane are parallel, including one from the vertex. The bottom (red) ray represents such a parallel ray, and it reflects off the vertex (which has a horizontal normal vector) to go upward by the same 9.574°. With this plane-wave assumption, we can then estimate each scatterer's QZ AoA as being equal to its geometric angle from the vertex. Note that a positive elevation incidence in the QZ is consistent with an upward look angle from the vertex. The QZ AoAs of strong stray signals from spectral analysis could then be compared with any potential scattering sources' predicted AoAs.

Figure 3 illustrates a scattering source well away from the focal point and off of the focal plane. One can readily see that the vertex ray bounces at a different angle than the ray to the probe in the QZ. In this example (and in most practical cases), the ray from the vertex with the QZ's "measured" elevation angle still comes close to the modeled scattering source. Note that if the scattering source were moved either direction along its upward ray toward the reflector, then the measured QZ elevation angle would remain the same, but the appropriate vertex angle would change.

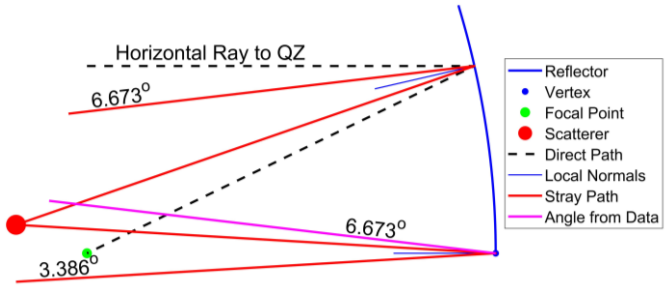

Figure 3 Geometry with scatterer behind focal plane.

For a more rigorous approach, one might compute geometries relative to a spot on the reflector in a direction from the QZ

closer to where those stray signals are detected. Two things (in addition to the range-feature locations) are needed: the Cartesian coordinates [X_r, Y_r, Z_r] and then spherical angles from the focal point [θ_r, ϕ_r] of that selected reflector spot and then the local normal $\vec{N}_\theta$. Identifying those values is fairly straightforward, but their use is not extensively explored here. First, pick a spot on the reflector at desired projected coordinates X_r and Y_r, where the focal point is the origin. It seems that the best choice of these coordinates would be a spot pointed to by a ray at the detected QZ AoA α from a QZ location that has strong spatial-frequency content with period $\lambda/\sin(\alpha)$. Given reflector coordinates (from the focal point) X_r, Y_r, and the focal length F, the quantities Z_r, θ_r, and ϕ_r will then be given by (1) – (3):

$$Z_r = F - \frac{(X_r^2 + Y_r^2)}{4F} \tag{1}$$

$$\theta_r = \text{atan}\left(\frac{\sqrt{(X_r^2 + Y_r^2)}}{Z_r}\right) \tag{2}$$

$$\phi_r = \text{atan2}(Y_r, X_r) \tag{3}$$

The local normal $\vec{N}_\theta$ will be in the direction [θ_r /2, ϕ_r] into those reflector coordinates. (The dashed line, horizontal vertex normal, and upper local normal in Figure 2 should provide a good visualization of this θ_r/2 relationship.) Once the location and attitude of that local normal are determined, then the locations of relevant range features in that frame would need to be converted to aspects that would be measured in the 1D or 2D field-probing scan.

The discussion above of elevation angles (obtained with probe rails at the plane-polar angle $\phi_p = 90°$ from horizontal) can be extended to other ϕ_p angles by rotating the hypothetical observer at the vertex by ϕ_p - 90° about the paraboloid's axis. The direction of forward probe travel represents the new "upward" direction when processing these other ϕ_p angles.

III. 1D Spectral Mapping

Other than the mapping of angles through a paraboloidal reflector discussed in Section II, the topic of mapping the directions to stray-signal sources from 2D QZ scanning has been covered in earlier works[1]. This section describes similar processing that can be applied to individual linear (1D) scans such as those on a conventional plane-polar field probe.

The automated output of this technique is fairly straightforward, as the output of a 1D FFT of lightly processed measured data consistent with that in 2D imaging. This output provides stray-signal strength, relative to the desired signal, vs. its arrival angle, relative to the plane normal to the scanning axis. The more tedious part is identifying potential scattering sources in the range, quantifying the angles where they would appear, and annotating the plot appropriately.

A. Example

Figure 4 shows the initial stray-signal map at several frequencies from 500 MHz to 2 GHz in a large compact range. This facility has a large feed carousel near the focal point, and a large absorber-covered enclosure around that carousel to hide it from the QZ. Figure 4 analyzes a vertical scan, such that the angles reported are elevation angles.

The first two range features to identify in a compact range are typically the reflector edges. Those are shown as black vertical lines in Figure 4 , and represent the nominal boundary between direct-path and reflected stray signals. (We suspected that those lobes within the reflector bounds are reflected because reflector anomalies would tend to get worse at higher frequency bands and these did not. Our suspicion was confirmed when improved absorber treatment near the annotated range features lowered those lobes.) The QZ angles to the reflected sources were estimated using the simple approach in Section II of finding the elevation angle from the reflector vertex. Drawings of the chamber layout were examined, and candidate scattering-source locations were identified and annotated with vertical lines and labels in Figure 4 .

We see that some range features in Figure 4 appear at multiple angles. These features are potentially visible directly from the QZ and/or bouncing off the reflector. Note that the reflection from the imaged focal point reports identically zero power due to the plane-wave-subtraction mechanism in use.

While three different angular regions showed significant stray-signal contributions, the worst (and thus the first) was deemed to be the image of the top front edge of the feed enclosure at about +10°. This was successfully addressed, and then other angular regions were addressed, testing the fixes with new scans run through this algorithm. After several iterations, the QZ ripple was deemed acceptable. Figure 5 shows the spectral stray-signal content after those several iterations, and it is significantly improved.

Note that if one does not have the range-layout drawings, or if those do not represent the current geometry (perhaps after several iterations of trying to fix the QZ ripple without this type of analysis tool), there may be an alternative way of finding a source. For those reported angles outside the reflector body, looking from the QZ center (or the spot in the QZ where that frequency of ripple seems to be the worst) in the reported direction should have you looking at the scattering source. For those reported within the reflector body, either:

- Point from the reflector vertex in the reported direction (either in-person or virtual), and you should be pointing close to the source.
    - Note that due to the conical ambiguity of a single linear scan[3], any point on a cone (with an axis parallel to the probe rails) of the reported angle would be equally plausible.
- Look from candidate sources to the vertex. If you have to look at the negative of the reported angle to see the vertex, then the feature at your observation point is a good candidate.

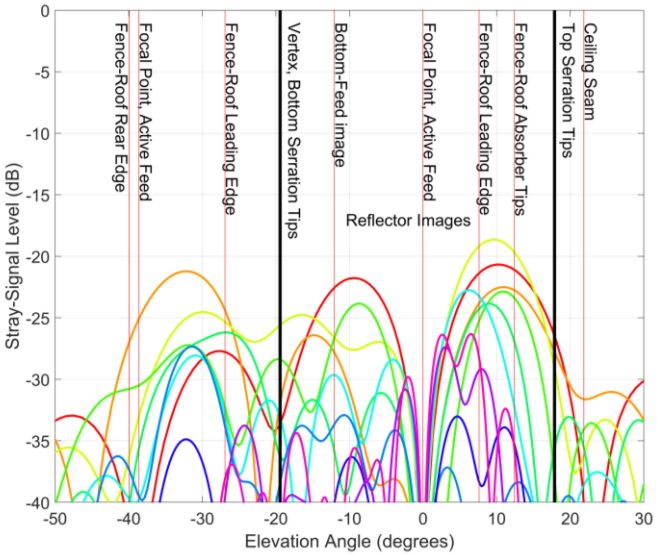

Figure 4 Initial stray-signal mapping.

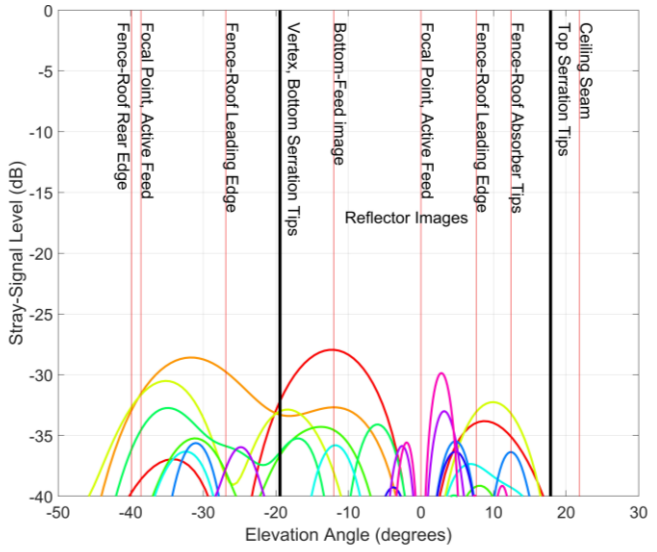

Figure 5 Final stray-signal mapping.

B. *Algorithm*

For a vertical scan of data as used in Figure 4 and Figure 5 , we start with measured complex voltage *v(y)* at a frequency with wavelength λ. The first step is typically to scale to and remove the primary plane wave[1][6]. In this example, the vertical probing rails were believed to be normal to the primary plane wave's direction, so the plane-wave contribution to the spectrum is estimated simply as the complex mean of *v(y)*. In (4) we then normalize *v(y)*, which will cause it to have unit mean, and then subtract that unit mean, leaving the complex stray-signal voltage $v_s(y)$ relative to the plane-wave strength.

$$v_s(y) = \mathrm{v(y)/mean(v(y))} - (1 + \mathrm{j0}) \qquad (4)$$

Note that if the probing rails were not normal to the range axis, as can often be the case in field probing, effectively subtracting the primary plane wave requires some extra steps:

- Unwrap the measured phase so that there are no jumps > +/-180°
- Find the best-fit line through that unwrapped phase, perhaps with the Matlab polyfit() function.
    - Note that stray signals from directions very close to the desired signal can corrupt this overall phase slope. Averaging primary AoA over frequency or ¼-wave Z shifts is often beneficial.
- Reconstruct the best-fit line at the measured scan positions, perhaps with Matlab's polyval() function. We will use this to steer and then perhaps countersteer the synthetic array of field-probe data.
- Subtract the line of phase from the measured phase
- Reconstitute the complex *v(y)* with this flattened phase and the original *v(y)* magnitudes
- Use (4) to subtract the primary plane wave to get $v_s(y)$
- If the range axis is a good reference for aspect angles, then add the line of phase back to $v_s(y)$. If not, then don't add the phase back in, and the normal to the probing rails will define 0°.

The next step is to define the sample set of the output, starting with its number of points. There is minimal penalty for choosing a large number of output points N_y, and 8K was the number used in the example.

Next, we will do a 1D FFT of the zero-padded v_s vector. We don't care about the phase of the spectral output, so no particular care is needed in the zero-padding mechanism (provided that the padding zeroes are inserted between the measured endpoints in the periodic transform input, as opposed to being inserted inside the measured data). One method is to create a new vector v_s' of length N_y and populate the beginning of it with v_s. Then we compute the plane-wave spectrum *S* using (5):

$$S = \frac{\mathrm{fftshift}\left(\mathrm{fft}(v_s')\right)}{N_m}, \qquad (5)$$

where N_m is the number of measured samples in *v(y)*.

The sine-space coordinates of the 1D FFT output with input spacing Δy and wavelength λ will be Ky/K from (6). Note that (6) assumes that N_y is chosen to be even.

$$Ky/K = \left(-\frac{N_y}{2} : \frac{N_y}{2} - 1\right) * \frac{\lambda}{N_y \Delta y} \qquad (6)$$

C. Notes

This algorithm assumes that the stray signal's contribution will be stationary over the scan extent. This might not be the case for near-field sources or for imaged sources that can only be seen during a portion of a scan due to occlusion or finite reflector size. If not stationary, the stray-signal strength may be underreported, and the direction might also be best interpreted from the scan location with the greatest perturbation rather than from the scan center.

IV. 1D Holographic Imaging

Many ranges have the potential for both plane-wave and spherical-wave stray signals. The compact range is one example, where bounces through the reflector discussed in Section II can be nearly planar waves, while other range features like the feed region will be much closer to the large QZ than the far-field distance. Spherical focusing[3] would be one approach to quantifying those potential close-in sources, but then the processing would require adjustment for each unique set of range features. Microwave holography[4] is a general technique that does not discriminate between near- and far-field radiation and makes no assumption about a stationary field. Its use of the FFT also makes it much faster than focusing to a densely populated area or volume.

Most microwave holography processes 2D input data on one plane and estimates the fields that would have been measured on other planes parallel to the first. That is not being done here. Instead, the technique described here starts with 1D data acquired along a line and produces a 2D image of that 1D line propagated by different radial distances.

Microwave holography is typically used in antenna testing to focus the antenna's plane-wave spectrum back to its aperture. There is an implicit assumption in that antenna-testing application that all radiation originates from that aperture. That assumption does not apply in this stray-signal application, where we're analyzing the spectrum of plane waves (including spherical waves) arriving at the QZ from all sources other than the one intended. Rather than looking for the field distribution where all radiators are known to be confined, we're looking in this application at hologram flow lines to estimate the strengths and locations of sources that are not the one desired plane wave.

A. Example

Figure 6 shows the output in dB of this 1D holography for a small compact range that had excessive QZ ripple. The input data were a single vertical line cut whose amplitudes are shown (after subtracting the primary plane wave[1][6]) at the left edge of the image. Those complex data were then propagated 100 times to the right edge of the image with a fixed positive propagation spacing Δz. The reflector, the feed, and an equipment enclosure behind the feed were then superimposed on the image. Figure 6 strongly suggests that the QZ ripple could be improved by addressing direct-path feed radiation and/or absorber treatment at the top edge of the equipment enclosure.

Figure 7 shows the same processing on data acquired after addressing the issues near the focal point. The resulting QZ ripple was within specifications, and Figure 7 suggests that radiation from near the focal point directly to the QZ is no longer a significant issue in this facility.

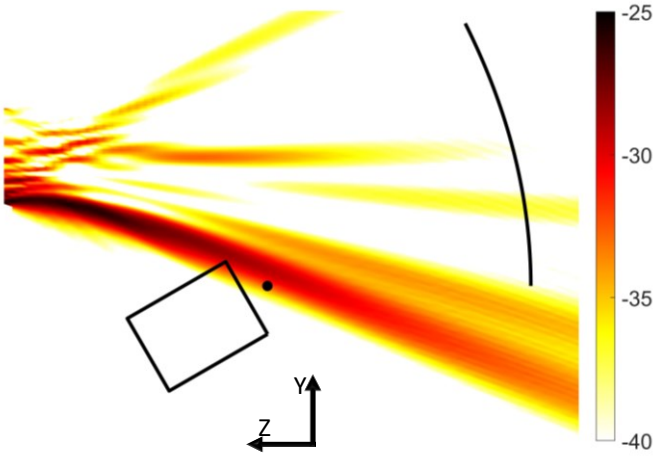

Figure 6 Initial stray-signal holographic image.

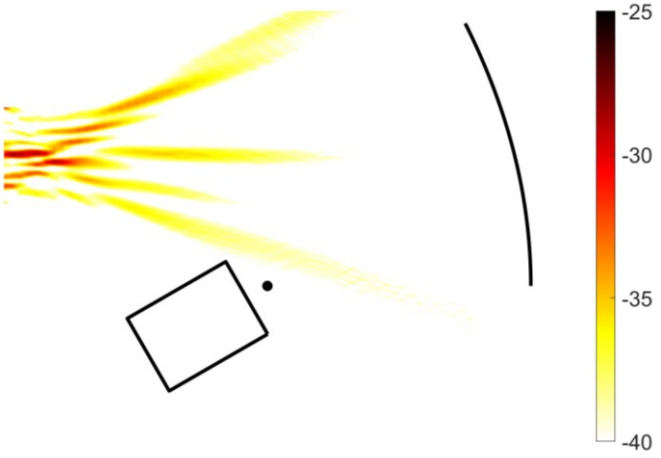

Figure 7 Hologram with final absorber configuration.

B. Algorithm

For a vertical line cut as used in Figure 6 , we start with measured complex voltage $v(y)$ at a frequency with wavelength λ. The first step is typically to scale to and remove the primary plane wave[1][6]. In this example, the vertical probing rails were again believed to be normal to the primary plane wave's direction, so we were again able to use (4) for normalizing to and removing the desired plane wave.

The next step is to define the image size desired, which will occupy an area $N_y\Delta y$ by $N_z\Delta z$ where Δy is the scan increment and the other three values are user-determined. This algorithm (in (6)) assumes that N_y is chosen to be even. A matrix of N_y rows and N_z columns is created to accumulate the image I. A vector of N_y points is created to initially hold the zero-padded FFT inputs and then the inverse-FFT outputs v'.

An N_y-length complex vector $P(Ky/K)$ is then defined for incremental spectral propagation. First, we need an N_y-length Kz

vector, which we arrive at from N_y, Δy, and λ. We'll be doing a 1D transform of an N_y-length vector (v') vs. y (in this example) with spacing Δy. We again find the vector Ky/K using (6). If we assume that $Kx/K = 0$, then the Kz vector is defined in (7) and the N_y-length spectral propagation vector P is defined in (8). Note that the fftshift() call in (4) is the only one required in this algorithm. Also note that P has been defined to have unit magnitude everywhere.

$$Kz = \text{fftshift}\left(\frac{2\pi}{\lambda}\sqrt{1-(Ky/K)^2}\right) \tag{7}$$

$$P = \begin{cases} e^{jKz\Delta z}, \left|\frac{Ky}{K}\right| \le 1 \\ 1 + \text{j}0, \left|\frac{Ky}{K}\right| > 1 \end{cases} \tag{8}$$

The next step is to populate the middle of vector v' at zero propagation with the complex stray-signal vector $v_s(y)$. Enough zeroes should exist on either side of $v_s(y)$ that the field can spread without aliasing the image's top into the bottom and vice versa. A new vector y' of size Ny should be defined as a superset of acquired y for plotting purposes with the acquired Δy and an offset that maintains the proper correlation between v' and y'. This vector v' has its magnitude copied into the first column of the output image I, and is also the initial input to the FFT in (9).

$$S = \text{fft}(v') \tag{9}$$

Now we loop iz from 2 to Nz, filling each column of image I. For each index iz, propagate spectrum S by another increment Δz in (10), and then update v' with the estimated spatial field vs. y' in (11). The $|v'|$ from (11) then fills the iz^{th} column of image I.

$$S = S \times P \tag{10}$$

$$v' = \text{fft}^{-1}(S) \tag{11}$$

C. Notes

With a 1D scan as input, the FFT output has conical ambiguity[3] about the scanning axis. The resulting image is then vs. cylindrical radius from the probe-aperture locus rather than vs. the down-range distance assumed here. The images in Figure 6 and Figure 7 show flow lines diverging at multiple angles from the scan axis, and one must be aware that those could represent stray signals at other cylindrical angles. In the example facility, the probability that significant stray signals were coming from cylindrical angles other than those close to downrange was low.

The described algorithm operates on a single (1D) scan of y. It could readily be adapted to operate on 2D input, extracting the desired 1D subset at each propagation interval. Visualizing all the 2D output would be a challenge, but 2D processing could overcome the conical ambiguity of the 1D output.

This algorithm assumes the use of a broad-beamed probe in order to avoid attenuating the stray signals we're looking for, and so that probe correction is not essential. Certainly, probe correction would be problematic in the 1D case if the stray signals were arriving from diverse (and unknown) angles about the scan axis.

For those strong flow lines that point toward the reflector, the ray tracing in Section II might be helpful in identifying the root cause. Since such a reflection would be a nearly planar phase front, and since the holography does not quantify AoAs, the spectral processing in Section III (operating on the same acquired data) seems better suited to analyzing those stray-signal paths.

V. Conclusions

A simple approximation for converting QZ AoA through a paraboloidal reflector to the corresponding reflector AoA was presented, with the QZ AoA simply used as the corresponding AoA at the reflector's vertex. This technique increases the utility of algorithms that do spectral processing of a compact range's QZ field, such as [1] and Sections III and IV. Two algorithms were also presented that help locate and quantify stray signals. Both use single scans that are often already being acquired for other purposes.

The algorithm in Section III does 1D plane-wave-spectral processing to estimate the strengths and AoAs of stray signals to the QZ. These AoAs can then be compared to known locations of suspected range features.

The algorithm in Section IV does microwave holography from the 1D scan to estimate the field magnitudes that would be measured at different radial distances from the single scan of data, with the hope that flow lines in the image will point in directions of near- or far-field stray-signal sources. This has proven useful when multiple close-in range features would be difficult to resolve with plane-wave-spectral processing.

These three techniques have been used with good success in multiple facilities to locate, quantify, address, and verify unwanted stray-signal sources. Before and after plots were shown for two facilities that used these tools, each with significant improvement.

References

[1] S. McBride and J. Hatzis, "Imaging a range's stray signals with a planar scanner", Proc. Antenna Measurement Techniques Association, 2018.

[2] S.T. McBride, "An efficient polar-coordinate Fourier-transform algorithm", IEEE-APS Symposium Digest, July,1992.

[3] S.T. McBride, "3D imaging of a compact range by focusing field probe data", Proc. Antenna Measurement Techniques Association, 1991, pp. 10A-27-32, October, 1991.

[4] J.C. Bennet, A.P. Anderson, P.A. McInnes, and A.J.T. Whitaker, "Microwave holographic metrology of large reflector anennas", IEEE Trans. Antennas Propagation, AP-24, pp. 295-303, 1976.

[5] S.T. McBride, "Focal-plane scanner for measuring radome beam deflection in a compact range", Proc. Antenna Measurement Techniques Association, 2008.

[6] Z. Chen, Z. Xiong and D. Lewis, "Direct wave removal in anechoic chamber range imaging from planar scanned data", 14th European Conference on Antennas and Propagation (EuCAP), Copenhagen, Denmark, 2020, pp. 1-5.